Flattening common image gathers after full-waveform inversion: the challenge of anisotropy estimation

Thibaut Allemand, Anna Sedova and Olivier Hermant, CGG*

Summary

Full-waveform inversion (FWI) is an unrivalled tool for velocity model building in areas covered by recorded reflected and diving waves. However, being driven mainly by the kinematics of diving waves, the resulting velocity models do not always flatten common image point gathers. This is generally interpreted as the result of poor estimation of the anisotropic parameters, arising even when multi-parameter anisotropic FWI is performed. Various regularizations can be introduced to mitigate the issue but fundamentally it should be solved by incorporating the kinematics of reflected waves. We propose a new approach involving a tilted transverse isotropic (TTI) joint reflected and diving ray tomography for estimating the initial anisotropic model for FWI. This step provides anisotropic parameters, which, for example, may then be kept fixed during FWI. The use of an original non-linear tomography algorithm for the joint reflected and diving rays is a key component for the efficiency and accuracy of our approach. We present here the algorithm and an application demonstrating the capability of the approach within a land FWI context on a full azimuth and ultra-long offset broadband dataset from the Sultanate of Oman.

Introduction

The estimation of an accurate velocity model of the subsurface is a crucial step in seismic imaging. In recent years FWI has become a well-established technique for velocity model building (see Virieux and Operto (2009) for a review). FWI can estimate both the long and short wavelength components of the velocity model in the area penetrated by diving waves, pushing the resolution beyond the capability of ray-based tomography.

However, it is often observed that common image point gathers (CIGs) depth-migrated using a velocity model updated with FWI are not flat, preventing a good focusing of the migrated seismic image (Mothi and Kumar, 2014). This is usually attributed to the improper estimation of anisotropy parameters. Indeed, FWI is mainly driven by the kinematics of diving waves, which travel nearly horizontally in the subsurface, while CIGs are computed using reflected waves, which travel more in the vertical direction. Therefore in an anisotropic medium, the velocity seen by diving and reflected waves may differ significantly.

Anisotropy estimation can be done through multi-parameter FWI. However, it is fundamentally an ill-conditioned problem. Some strategies have been proposed to tackle it. Among them, Stopin et al. (2014) use a strong regularization on the anisotropy parameter to improve the conditioning of the inversion; Debens et al. (2015) use a global optimization scheme for a smooth anisotropy parameter coupled with a local optimization for the velocity; Cheng et al. (2014) switch to multi-parameter inversion only when velocity-only inversion has stabilized.

Improving the conditioning of joint velocity and anisotropy inversion can actually only be done if diving and reflected waves are handled simultaneously. A heuristic method to do so consists of alternating steps of ray-based tomography and FWI, the classical workflow being the sequence tomography-FWI-tomography (Mothi and Kumar, 2014). In this sequential approach, in the area investigated by diving waves, FWI provides the high resolution velocity model, while tomography provides the extra information necessary for assessing anisotropy. However, strong coupling of velocity and anisotropy parameters makes convergence challenging. We believe that this problem can be solved more efficiently using a ray-based approach that directly combines both types of waves in a non-linear way. This should be used as a prior step to FWI allowing the estimation of the anisotropic parameters that are then fixed during the FWI update, or provide a much better starting point for multi-parameter FWI. The idea of using ray-based techniques to estimate the anisotropy prior to FWI is not new, see for example Qin et al. (2014) or Xie et al. (2017), but the use of a non-linear approach combining picks from reflected and diving waves makes it particularly accurate and efficient (Prieux et al., 2012).

In the following sections we first present the method and then apply it on a 3D land dataset to show its ability to recover both diving wave kinematics and CIG flattening. Finally, we discuss the results obtained using the joint tomography-FWI workflow.

Joint reflection-diving ray tomography

While traveltime tomography of diving waves can be easily implemented in a non-linear way (Taillandier et al., 2011), with first break times picked from shot or receiver gathers and then used in an iterative scheme to update the velocity model, most ray-based migration velocity analysis tools are only able to provide a linear update after each dip and residual move-out (RMO) picking step (Woodward et al., 2008). Therefore, non-linear slope tomography (Guillaume et al., 2008), with its non-linear forward modeling functionality, offers a tremendous advantage for the combination with diving ray tomography.

The core of this non-linear tomography is the use of the so-called kinematic invariants, which represent the kinematic characteristics of locally coherent events in the un-migrated domain. They are generally obtained through a kinematic demigration of dip and RMO picks in the pre-stack depth migration domain. They are then used to feed a non-linear iterative algorithm involving kinematic migrations and updates of the velocity model in order to minimize the slope of RMO (Montel et al., 2009).

We propose to combine this with diving ray tomography, which can be seen as a ray-based version of diving wave FWI, taking advantage of the non-linear capabilities of the two methods. The associated joint cost function can be expressed as

$$C(m) = \sum_{i=1}^{N_{RMO}} a_i |dRMO_i|^l + w \sum_{j=1}^{N_{FB}} b_j |\Delta t_j|^l + R(m)$$

where N_{RMO} and N_{FB} are the number of picked reflected events and the number of picked first breaks, respectively; $dRMO$ is the slope of the reflected event in the CIG (derivative of the depth position with respect to the CIG parameter, namely offset or angle); Δt is the traveltime misfit (difference between computed time in the current model and picked traveltime on the data); a_i and b_j are weights on each data (they can be offset-based or include a data quality factor, for example); w is a global weight applied to diving ray misfit term; l describes the chosen norm, and finally $R(m)$ stands for additional constraint and regularization terms applied to the model (including Tikhonov type, or Laplacian, in particular), that are required in every ill-posed inverse problem.

The cost function is minimized through a non-linear iterative multi-scale procedure. The first step involves a kinematic migration which allows re-localizing the invariants in the updated velocity model. Then Fréchet derivatives, with respect to the model parameters, are computed and the model perturbation is found by solving the normal equations of the least squares problem using an iterative linear solver.

Dealing with anisotropy

Our approach aims at estimating accurately the anisotropy parameters for the later FWI update. In a tilted transverse isotropic (TTI) medium with known tilt angles, there are three unknowns: the velocity along the principal symmetry axis V_v and, the anisotropy parameters ϵ and δ, following Thomsen (1986). In practice, we commonly assume that the tilt angles follow the structures of the migrated image.

Kinematic migration of reflected events in an anisotropic medium does not bring much complexity with respect to the isotropic case. First breaks are usually modeled by solving the Eikonal equation, which provides a more stable solution than ray tracing. However, solving the anisotropic Eikonal equation can be computer intensive. Here we split first break modeling into two steps. First, we solve the isotropic Eikonal equation $|\nabla T|^2 = 1/V_h^2$ for each source using the horizontal velocity $V_h = V_v\sqrt{1+2\epsilon}$. This gives an approximated traveltime map. A trajectory between source and receiver is computed following the traveltime gradients. Then we perturb this trajectory using a ray bending algorithm to get rays that satisfy Fermat's principle in the full anisotropic model.

Which parameters should we invert for? Several studies deal with sensitivity analysis. Djebbi et al. (2017) compute the traveltime sensitivity kernels in a VTI context for several parameterizations. They conclude that diving waves are mostly sensitive to the horizontal velocity V_h whereas reflections are mostly sensitive to the NMO velocity $V_{NMO} = V_v\sqrt{1+2\delta}$. When diving waves and reflections are used simultaneously, they suggest to use (V_{NMO}, η, δ), where the anellipticity parameter is defined by $\eta = \frac{\epsilon-\delta}{1+2\delta}$. It was demonstrated that we cannot recover the three parameters using surface P-wave seismics only in layered models (Alkhalifah and Tsvankin, 1995). Usually, δ is derived from, or constrained by, well data or regional geological knowledge, while V_v and ϵ are estimated keeping δ fixed (or obeying a priori rock physics-based relationship between ϵ and δ). In the example below, we choose to keep δ fixed during the tomography. In this case, solving for (V_v, ϵ) or (V_{NMO}, η) does not make much difference, and we choose the former for simplicity. We allow long wavelength spatial variations only for ε in order to mitigate the tradeoff between anisotropy and velocity (as Stopin et al., 2014).

Additionally, the computation of the Fréchet derivatives gives access to the Gauss-Newton approximation of the Hessian, which is used to precondition the gradient and limit the crosstalk between parameters.

Land 3D field example

We tested our method on a 3D land broadband wide azimuth vibroseis dataset from the Sultanate of Oman (Mahrooqi et al., 2012), with a 9 s sweep from 1.5 to 86 Hz. The acquisition design is 50 m by 50 m interval for the shots, and 250 m by 25 m interval for the receivers. A full time and depth processing project has been completed on this dataset, without FWI, using multi-layer TTI reflection tomography. In the example shown here we work on a subset area of 800 km^2 on which an FWI study has been conducted recently (Sedova et al., 2017).
First breaks were picked up to 10 km offset, while RMO picks were available from the recently completed depth

processing project. Two wells are located in the center of the study area. We computed an initial velocity model by smoothing the pre-stack time migration (PreSTM) RMS velocities in the time domain and converting them to interval velocities in the depth domain. The initial anisotropy parameters were constant: $\epsilon = 12\%$ and $\delta = 5\%$, coming from known regional values.

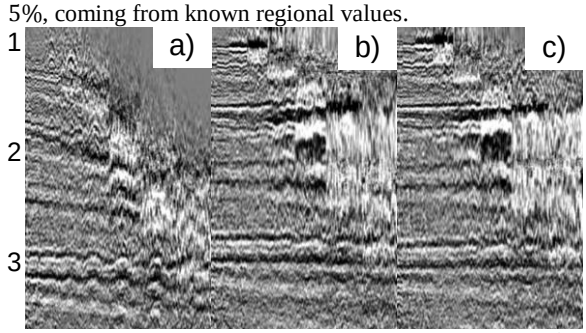

Figure 1: Common image point snail gathers migrated in depth for: a) initial model, b) reflection tomography model, and c) joint reflection-diving ray tomography model. The vertical scale is in km and the offsets are from 0 to 4 km.

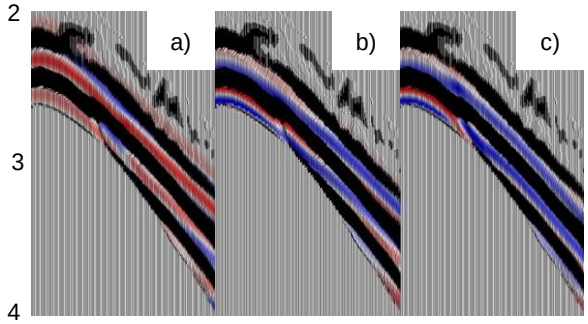

Figure 2: Common receiver gathers. Real data (black wiggles) are overlaid on synthetic data (blue/red) computed using: a) initial model, b) reflection tomography model, and c) joint reflection-diving ray tomography model. The vertical scale is in seconds and the offsets are from 3.8 km to 10 km. Black wiggles should overlap with red: a perfect QC should show black and blue only.

We ran two tomography tests updating jointly V_v and ϵ starting from the same initial model: the first time using reflections only, and the second time using reflections and first breaks jointly. CIGs and wave equation modeled diving wave synthetics are shown in Figure 1 and Figure 2, respectively. Reflection tomography and joint reflection-diving ray tomography both achieve a good flattening of the CIGs, but only the latter also correctly models the diving wave kinematics. This gives us good confidence in the method: flat CIGs and honored first break traveltimes mean that the estimated V_v and ϵ are reliable.

Using joint tomography as a starting model for FWI

We now use the joint reflection-diving ray tomography to build a starting model for FWI. Starting from the PreSTM-derived depth model, and using the aforementioned constant anisotropy, we perform a first pass of joint tomography to update V_v and ϵ. Then we update V_v and δ using well data extrapolated along two horizons, and we perform a second pass of joint tomography for both V_v and ϵ. The ε and δ models after joint tomography are shown in Figure 3, overlaid on a migrated stack section. The output model is used as an input to FWI inverting both diving waves and reflections from 3 Hz up to 13 Hz, for updating V_v only. The preprocessing applied to the data prior to FWI is the same as in Sedova et al. (2017). We observe on Figure 4 that the convergence of diving wave FWI is improved when we start from the joint tomography model rather than the simpler initial model, especially at near offsets, due to the better estimation of anisotropy.

To QC our final result after the FWI at 13 Hz, we compare in Figure 5 a CIG computed in the legacy multi-layer TTI reflection tomography model with the same CIG computed in FWI model. We clearly see a reduction of wobbling across offsets and an overall satisfactory flatness of events. We also observe good agreement between the velocity model and the well log. Synthetics overlaid on the real seismics are shown in Figure 6 for the same two models. Unsurprisingly, the match between synthetics and real data is better after FWI than after reflection tomography, and the modeling using the FWI model is able to reproduce more events. Hence described approach allows honoring both the reflections and the diving wave kinematics, and matching well data.

Finally, three depth slices of the final velocity model overlaid on seismics are displayed in Figure 7 together with an inline section. FWI has recovered fine details like near surface channels and faults that nicely match with the seismics.

Conclusion

We presented a joint reflection-diving ray tomography that allows the recovered anisotropy to be used in FWI. We applied it to a real land dataset from the Sultanate of Oman. Computed FWI model gives an excellent match between synthetic and real data, especially at long offsets. It flattens the CIGs and the vertical velocity profile compares nicely with the well log, demonstrating the capability of the method.

Acknowledgements

We acknowledge PDO and the Ministry for Oil and Gas of the Sultanate of Oman for permission to use the data. We thank our colleagues Gilles Lambaré and Patrice Guillaume for many helpful discussions, and CGG for permission to publish this work.

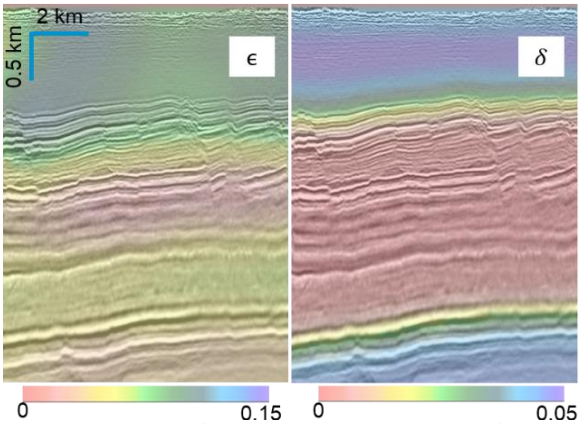

Figure 3: Epsilon (left) and delta (right) models after joint reflection-diving ray tomography.

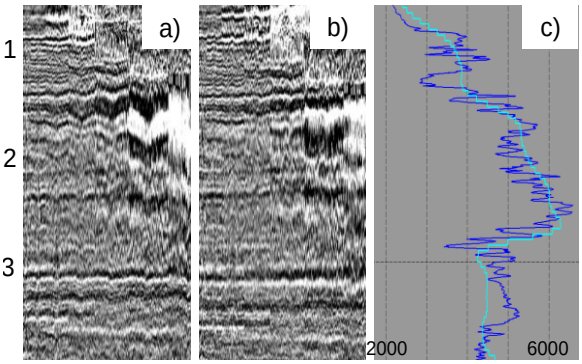

Figure 5: a) Snail CIG in legacy tomography model, b) snail CIG in FWI model, and c) comparison to well log: cyan is FWI, blue is the well log. The vertical scale is depth in km. Offset is from 0 to 4 km; velocity is in m/s.

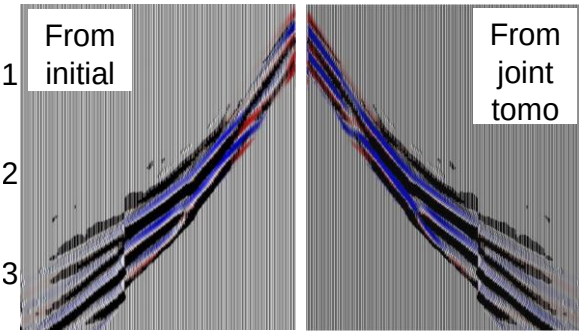

Figure 4: Common receiver gathers displayed back to back. Real data filtered at 9Hz (black wiggles) is overlaid on synthetics (blue / red) computed using: left) 9 Hz FWI from initial model, and right) 9 Hz FWI from joint reflection-diving ray tomography model. The vertical scale is in seconds, offsets are from 0 to 8 km.

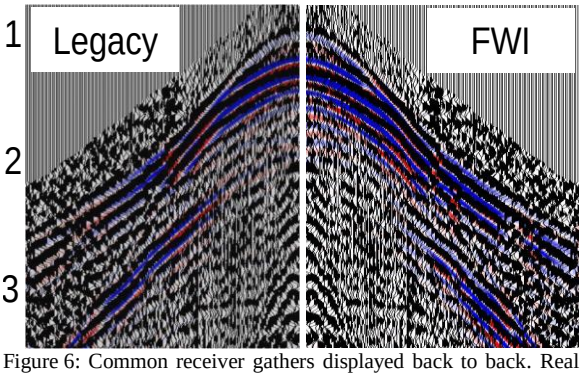

Figure 6: Common receiver gathers displayed back to back. Real data (black wiggles) is overlaid on synthetics (blue / red) computed using: left) legacy multi-layer tomography model, right) 13 Hz FWI model. The vertical scale is in seconds and the offsets are from 2 to 8 km. Black wiggles should overlap with red.

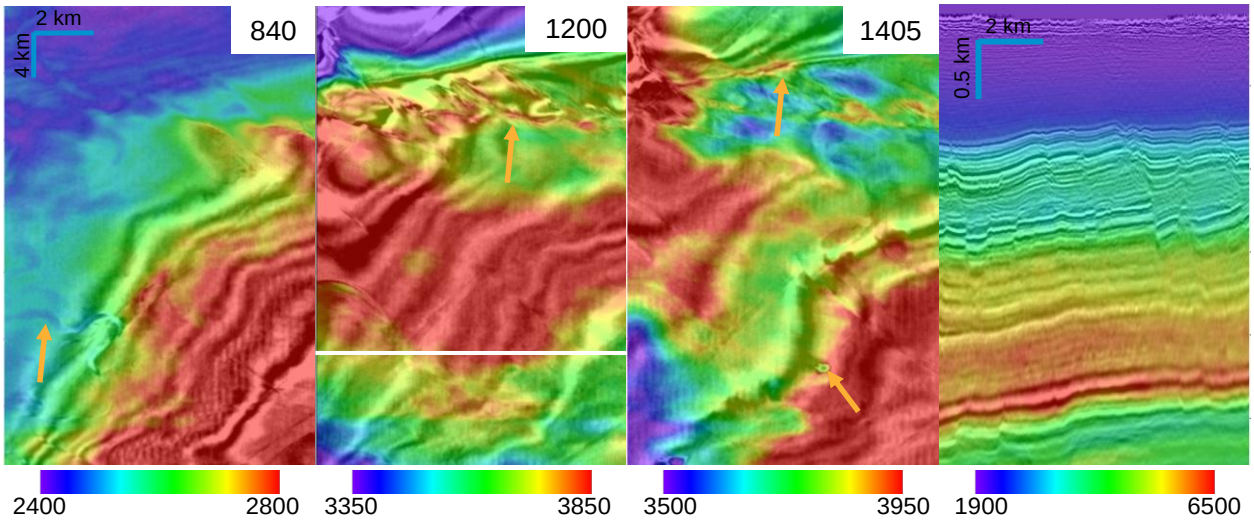

Figure 7: The three left panels are depth slices of velocity after 13 Hz FWI overlaid on seismics. The depth in meters is indicated in the top right corner of each panel. The velocity is in m/s. The right panel is an inline section of the velocity overlaid on the seismic stack. The white line in the second panel indicates the position of the inline section.

EDITED REFERENCES

Note: This reference list is a copyedited version of the reference list submitted by the author. Reference lists for the 2017 SEG Technical Program Expanded Abstracts have been copyedited so that references provided with the online metadata for each paper will achieve a high degree of linking to cited sources that appear on the Web.

REFERENCES

Alkhalifah, T. and I. Tsvankin, 1995, Velocity analysis for transversely isotropic media: Geophysics, 60, 1550–1566, http://dx.doi.org/10.1190/1.1443888.

Cheng, X., K. Jiao, D. Sun, and D. Vigh, 2014, Anisotropic parameter estimation with full-waveform inversion of surface seismic data: 84th Annual International Meeting, SEG, Expanded Abstracts, 1072–1077, https://doi.org/10.1190/segam2014-0821.1.

Debens, H. A., M. Warner, A. Umpleby, and N. V. da Silva, 2015, Global anisotropic 3D FWI: 85th Annual International Meeting, SEG, Expanded Abstracts, 1193–1197, http://dx.doi.org/10.1190/segam2015-5921944.1.

Djebbi, R., R.-É. Plessix and T. Alkhalifah, 2017, Analysis of the traveltime sensitivity kernels for an acoustic transversely isotropic medium with a vertical axis of symmetry: Geophysical prospecting, 65, 22–34, http://dx.doi.org/10.1111/1365-2478.12361.

Guillaume, P., G. Lambaré, O. Leblanc, P. Mitouard, J. Le Moigne, J.-P. Montel, T. Prescott, R. Siliqi, N. Vidal, X. Zhang, and S. Zimine, 2008, Kinematic invariants: an efficient and flexible approach for velocity model building: 78th Annual International Meeting, SEG, Expanded Abstracts, 3687–3692, http://dx.doi.org/10.1190/1.3064100.

Mahrooqi, S., S. Rawahi, S. Yarubi, S. Abri, A. Yahyai, M. Jahdhami, K. Hunt, and J. Shorter, 2012, Land seismic low frequencies: Acquisition, processing and full wave inversion of 1.5-86 Hz: 82nd Annual International Meeting, SEG, Expanded Abstracts, 1–5, http://dx.doi.org/10.1190/segam2012-0961.1.

Montel, J.-P., N. Deladerriere, P. Guillaume, G. Lambaré, T. Prescott, J.-P. Touré, Y. Traonmilin, and X. Zhang, 2009, Kinematic invariants describing locally coherent events: an efficient and flexible approach to non linear tomography: 71st Annual International Conference and Exhibition, EAGE, Extended Abstracts, Workshop WS 1: Locally Coherent Events–A New Perspective for Seismic Imaging.

Mothi, S., and R. Kumar, 2014, Detecting and estimating anisotropy errors using full waveform inversion and ray-based tomography: A case study using long-offset acquisition in the Gulf of Mexico: 84th Annual International Meeting, SEG, Expanded Abstract, 1066–1071, http://dx.doi.org/10.1190/segam2014-0324.1.

Prieux, V., G. Lambaré, S. Operto, and J. Virieux, 2013, Building starting model for full waveform inversion from wide-aperture data by stereotomography: Geophysical Prospecting, 61, 109–137, http://dx.doi.org/10.1111/j.1365-2478.2012.01099.x.

Qin, B., V. Prieux, H. Bi, A. Ratcliffe, J.-P. Montel, D. Carotti, and G. Lambaré, 2014, Towards high-frequency full waveform inversion-A Case Study: 76th Conference and Exhibition, EAGE, Expanded Abstracts, We E106 07, http://dx.doi.org/10.3997/2214-4609.20141086.

Sedova, A., G. Royle, O. Hermant, M. Retailleau, and G. Lambaré, 2017, High-resolution land full-waveform inversion: a case study on a data set from the Sultanate of Oman: 79th Conference and Exhibition, EAGE, Expanded Abstracts, http://dx.doi.org/10.3997/2214-4609.201701163.

Stopin, A., R.-É. Plessix, and S. Al Abri, 2014, Multiparameter waveform inversion of a large wide-azimuth low-frequency land data set in Oman: Geophysics, 79, WA69—WA77, http://dx.doi.org/10.1190/geo2013-0323.1.

Taillandier, C., N. Deladerrière, A. Therond, and D. Le Meur, 2011, First arrival traveltime tomography-when simpler is better: 73rd Conference and Exhibition, EAGE, Expanded Abstracts, http://dx.doi.org/10.3997/2214-4609.20149305.

Thomsen, 1986, Weak elastic anisotropy: Geophysics, 51, 1954—1966, http://dx.doi.org/10.1190/1.1442051.

Virieux, J., and S. Operto, 2009, An overview of full-waveform inversion in exploration geophysics: Geophysics, 74, no. 6, WCC1–WCC26, http://dx.doi.org/10.1190/1.3238367.

Woodward, M. J., D. Nichols, O. Zdraveva, P. Whitfield, and T. Johns, 2008, A decade of tomography: Geophysics, 73, no. 5, VE5–VE11, http://dx.doi.org/10.1190/1.2969907.

Xie Y., B. Zhou, J. Zhou, J. Hu, L. Xu, X. Wu, N. Lin, F. C. Loh, L. Liu, and Z. Wang, 2017, Orthorhombic full-waveform inversion for imaging the Luda field using wide-azimuth ocean-bottom-cable data: The Leading Edge, 36, 75–80, http://dx.doi.org/10.1190/tle36010075.1